International Journal of Neural Systems (2021)
Author Preprint
DOI: 10.1142/S0129065721500349

Galvanic Vestibular Stimulation-Based Prediction Error Decoding and Channel Optimization

Yuxi Shi[*,‖], Gowrishankar Ganesh[†,‡,**], Hideyuki Ando[§,††], Yasuharu Koike[¶,‡‡], Eiichi Yoshida[‡,§§] and Natsue Yoshimura[¶,¶¶]

[*]*School of Engineering, Tokyo Institute of Technology*
2-12-1 Ookayama, Meguro-ku, Tokyo, 152-8550, Japan

[†]*CNRS (Centre National de la Recherche Scientifique)*
Universite Montpellier (UM) Laboratoire de Informatique
de Robotique et de Microelectronique de Montpellier (LIRMM)
Montpellier, France

[‡]*CNRS-AIST JRL (Joint Robotics Laboratory)*
IRL3218, National Institute of Advanced Industrial Science and Technology
Tsukuba Central 1, 1-1-1 Umezono, Tsukuba 305-8560, Japan

[§]*Graduate School of Information Science and Technology, Osaka University*
2-1 Yamadaoka, Suita, Osaka 565-0871, Japan

[¶]*Institute of Innovative Research, Tokyo Institute of Technology*
2-12-1 Ookayama, Meguro-ku, Tokyo 152-8550, Japan

[‖]*shi.y.ac@m.titech.ac.jp*
[**]*Ganesh.Gowrishankar@lirmm.fr*
[††]*hide@ist.osaka-u.ac.jp*
[‡‡]*koike@pi.titech.ac.jp*
[§§]*e.yoshida@aist.go.jp*
[¶¶]*yoshimura@pi.titech.ac.jp*

Received 10 May 2021
Accepted 11 May 2021
Published Online

A significant problem in brain–computer interface (BCI) research is decoding — obtaining required information from very weak noisy electroencephalograph signals and extracting considerable information from limited data. Traditional intention decoding methods, which obtain information from induced or spontaneous brain activity, have shortcomings in terms of performance, computational expense and usage burden. Here, a new methodology called prediction error decoding was used for motor imagery (MI) detection and compared with direct intention decoding. Galvanic vestibular stimulation (GVS) was used to induce subliminal sensory feedback between the forehead and mastoids without any burden. Prediction errors were generated between the GVS-induced sensory feedback and the MI direction. The corresponding prediction error decoding of the front/back MI task was validated. A test decoding accuracy of 77.83–78.86% (median) was achieved during GVS for every 100 ms interval. A nonzero weight parameter-based channel screening (WPS) method was proposed to select channels individually and commonly during GVS. When the WPS common-selected mode was compared with the WPS individual-selected mode and a classical channel selection method based on correlation coefficients (CCS), a satisfactory decoding performance

[¶¶]Corresponding author.

of the selected channels was observed. The results indicated the positive impact of measuring common specific channels of the BCI.

Keywords: Electroencephalogram; galvanic vestibular stimulation; prediction errors; motor imagery; channel optimization; brain-computer interface.

1. Introduction

Globally, particularly in developed countries, the numbers of senior citizens and persons with varying degrees of disability,[1,2] who struggle to control their limbs and other body parts,[3] are increasing. Therefore, wheelchairs have become one of the most important methods of transportation.[1,4] However, existing wheelchairs, such as mechanical wheelchairs are difficult for such people to control.[4] Hence, brain–computer interface (BCI) technologies are promising because they can enable people to control wheelchairs with their brains instead of their bodies. This could be useful for providing alternative communication and mobility to assist elderly or disabled people and aid them in regaining more independence in their daily activities.[5] BCI technologies are also evolving to provide therapeutic benefits by inducing cortical reorganization via neuronal plasticity for the neurological disorders.[6]

Researchers have studied inducible BCI systems[7–9] that depend on the participants sensory pathway, which is induced by an explicit external stimulation.[10–12] According to the form of stimulation, these can be divided into visually evoked potentials, auditory evoked potentials and tactile evoked potentials. As the inductive BCI system requires additional stimulation devices and the users attention, it results in a cognitive load for the users.[13] However, the spontaneous BCI system is completely derived from the participant's inherent brain signals.[14–16] Although it provides a more flexible and natural control method, some cases still require extensive user training, either to enable the user to control their brain activity[17,18] or for the motor imagery (MI).[8,9,19] Some imagery differs with the user who wants to control the BCI system. Therefore, users still bear some usage burden.

In our previous study,[20] a new methodology was explored for decoding whether the movement that users imagined matches the sensory feedback induced by a subliminal stimulator. This differs from the previously proposed methods that directly decode the motor imaginations of the users. This methodology is motivated by the well-documented ability of the brain, to use forward models[21] for predicting the sensory outcomes of self-generated and imagined actions. The sensory prediction errors generated between the forward model prediction and the actual sensory signal are the basis of social motor ability,[20] and can be generated during the period of real motion and during the MI period.[22,23] Prediction errors are considered to correspond to the control of self-generated actions,[21,24,25] haptic perception,[26] motor learning,[27] and even interpersonal interactions[28–30] and self-cognition.[31]

In previous studies, by using single-channel galvanic vestibular stimulation (GVS),[32–34] a form of subliminal stimulation (max 0.8 mA), designed to induce sensory feedback (left/right roll) was used. Meanwhile, the participants were requested to perform MI as if they were in a wheelchair and turning left/right, thus producing prediction errors that corresponded to the direction of the MI and the sensory feedback of the GVS. Better decoding performance across the tested participants was observed in the decoding of the left/right MI task within 96 ms of the stimulation (also satisfactorily decoded in other processing periods of the GVS-induced prediction errors).

The multichannel GVS-induced prediction errors in the front/back MI task were not verified in the previous study. However, for planar motion control of the wheelchair, the four principal directions left/right/front/back must be decoded. The decoding procedures were split into two sides: left/right and front/back, and a corresponding decoding method that can be used in real-time wheelchair control was considered (see Fig. 1). As the intention of MI cannot be observed in advance, the GVS stimulation was applied every 100 ms for measuring and decoding convenience in four directions: left, right, front and back. The users could perform MI freely in each 1 s period, and the decoding process was conducted eight times at intervals of 100 ms during

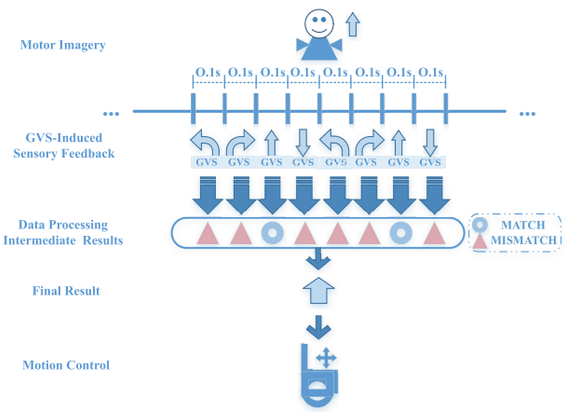

Fig. 1. Hypothetical EEG-controlled wheelchair.

this 1 s period. The final decoding result was decided based on the average decoding results of the trials.

Hence, the experimental settings were partially modified according to the actual requirements for hypothetical wheelchair control. Furthermore, the main focus was the prediction error decoding of the front/back MI task (the left/right MI task was not repeated in detail, and wheelchair control was not involved). A four-channel GVS device[35] was used, with a lower level of current stimulation (max 0.4 mA, half of the stimulation applied in the previous research), namely noninductive subliminal stimulation, which was applied across the vestibular-temple organs of the participants and induced the sensory feedback of a front/back pitch, leading to the generation of prediction errors without any stimulation load. Satisfactory decoding performance was achieved in this study.

In addition, as the signals of some channels may contain redundant information and noise that degrade BCI performance,[36] when designing applications of real-time BCI, equipment, costs, and decoding expenses should also be considered. The preferred decoding system is one that allows users to acquire sufficient information from limited data. Therefore, during the GVS-induced period, after decoding, the weight parameter output vector (characterizing the contribution of each channel's feature value to the decoding) was analyzed. The count values of the nonzero weight parameters of each channel were calculated, and then all the channels were sorted by descending order of count values. We referred to this method as the weight-parameter-based channel screening (WPS) method.

This method was utilized in the channel selection by participants individually (individual-selected mode). To verify whether all participants could share the common selected channels, we comprehensively analyzed the weight parameter output vector and calculated the count values of all channels across the participants (common-selected mode). Then, the channels were arranged in descending order. By processing the data of these top channels rather than all 64 channels, a better decoding performance could be observed; moreover, the decoding cost was reduced. To verify the efficacy of our proposed method, the WPS was compared with another proposed CCS method[36,37] under the common-selected mode.

2. Materials and Methods

2.1. *Participants*

Ten healthy participants (8 males, 2 females aged 2125 years) were included in our experiments. They were all dextromanuals and fully capable. The participants signed a written informed consent form before participating. The study was conducted with the approval of the ethics committee at the Tokyo Institute of Technology in Tokyo, Japan.

2.2. *Electroencephalogram (EEG) signal recording*

A commercial EEG recording system (Active Two amplifier system, 64 active sensors, BIOSEMI) recorded the brain activity at 2048 Hz. The National Instruments-6259 transmitted the trigger signals, and stereo speakers provided the audio cues to indicate the direction that the participants should imagine.

2.3. *GVS stimulation*

A custom-made GVS[35] was used in parallel with the EEG recording. The GVS instrument had four electrode sockets, each of which was connected to a separate constant current source circuit that provided stable current. Each circuit was insulated to prevent current flow between the various circuits. The GVS instrument was connected to a computer via USB 3.0, and the corresponding control command was issued by the computer to control the loop current of each circuit.

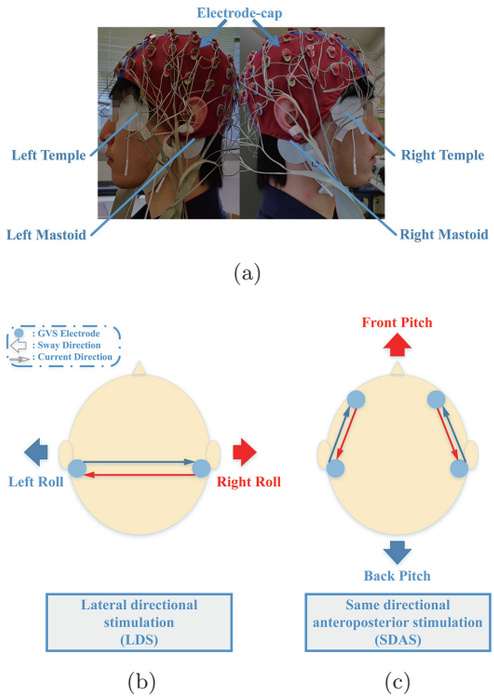

Fig. 2. Positions and current paths of the GVS electrodes.

As shown in Fig. 2(a), the four electrodes were attached to each participants left/right temple and mastoid. In this study, the lateral directional stimulation (LDS) and same directional anteroposterior stimulation (SDAS) methods[35] were used to induce sensory feedback. In LDS, the current flows from an electrode on either the left or right mastoid to the other mastoid. As shown in Fig. 2(b), the blue current pathway from the left mastoid to the right mastoid evokes the left roll sensation. Similarly, the red current pathway from the right mastoid to the left mastoid evokes the right roll sensation. In SDAS, the current is induced from electrodes on either of the temples or the mastoids and exits from the electrodes on the other regions. As shown in Fig. 2(c), the red current flowing from both sides of the temples to the mastoids evokes the front pitch sensation. Similarly, the blue current flowing from both sides of the mastoids to the temples evokes the back-pitch sensation.

2.4. *Experiment setup*

In the electrode setup, the skin was first cleaned to ensure that the participant would not feel the current stinging during the experiment. Then, the GVS electrodes were attached, and the current value of the GVS electrodes was adjusted according to the participants feedback. They answered questionnaires according to the perception of the test GVS stimulus from 1 to 8 (1: no feeling). The test GVS stimulus was set to a maximum current of 0.4 mA and 0.5 s of a 1 Hz sine wave was applied (the stimulation paradigms were LDS and SDAS), and the participants were exposed to the stimulus twice for each of the four GVS directions. After that, the participants were fitted with an electrode-cap and the electrodes were attached (see Fig. 2(a)).

During the experimental guidance, we moved the participants into a shielded room and placed them in a revolving office chair. To familiarize the participants with the MI (as if in a wheelchair and moving forward/backward), we asked them to close their eyes and feel the forward/backward movement. After that, before officially starting the experiment, several trials were conducted for the participants could to enter the experimental state as quickly as possible.

The participants were requested to keep their eyes closed and maintain calm for the duration of the experiment. See the timeline shown in Fig. 3(a). The participants imagined the motion according to random voice cues (front or back). Three seconds later, the GVS device stimulated the participants randomly with sensory feedback from four directions: left/right (LDS) and front/back (SDAS) by using sine wave stimulation (1 Hz, max 0.4 mA, sustained 0.5 s). After that, the participants were cued by a beep to rest for 3 s. The trials were repeated 60 times.

In this study, each volunteer participated in an experiment consisting of six sessions, where every session contained 60 trials. As the trial setting in Fig. 3(b) shows, the direction of the cue ("C") was front ("F") or back ("B"), and the sensory feedback directions of the GVS ("G") device were left ("L"), right ("R"), front ("F"), or back ("B"), giving 2×4 combinations for the cue and GVS stimuli. For example, CFGB means that the cue direction is at the front, and the GVS-induced sensation is at the back. MATCH means that the direction of the cue matches the GVS direction and consists of 15 trials in each of the following cases (a total of 30 trials): CFGF and CBGB. MISMATCH means that the direction of the cue does not match the GVS direction and consists of five trials in each of the following cases (totaling

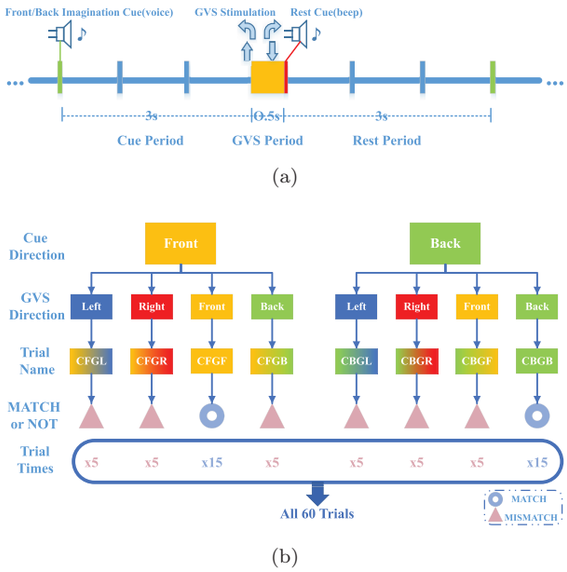

Fig. 3. (Color online) Timeline and trial settings of the experiment. (a) Experimental timeline: in each trial, the speakers give random voice cues to participants. Three seconds later the GVS device stimulates the participants for 0.5 s. Participants should make the MI before hearing the rest cue and then take a 3 s rest period; (b) Experiment trial setting: the four GVS cue initials and the related directions are used to abbreviate the trial name. When the cue and GVS directions are the same, it represents a MATCH (two types, each containing 15 trials) and is marked by a blue circle; otherwise, it represents a MISMATCH (six types, each containing 5 trials) and is marked by a red triangle.

30 trials): CFGL, CFGR, CFGB, CBGL, CBGR and CBGF. Similarly, in the left/right MI task, the direction of the cue ("C") was left ("L") or right ("R"). The sensory feedback directions of the GVS were also from four directions. The cases for MATCH consisted of CLGL and CRGR, and those of MISMATCH consisted of CLGR, CLGF, CLGB, CRGL, CRGF and CRGB (the processing will be explained mainly in the front/back MI task).

2.5. *Data processing*

Considering the applications of real-time BCI, data closer to the raw state were used for decoding analysis in this study. The main procedures of the data processing program were as follows (cue period: 3 s only MI period; GVS period: 0.5 s period in which GVS was applied to induce the sensory feedback):

(1) The EEG data were downsampled to 512 Hz.

(2) The downsampled data were divided into the cue and GVS periods. In the cue period, the data were separated and labeled as different datasets according to whether the direction of the MI was front or back. In the GVS period, according to whether the induced sensory feedback of GVS was equal to the direction of the cue, the data were separated into MATCH and MISMATCH datasets (see Experimental setup in detail) and labeled. Then, the mean amplitude value of the last 100 ms of the cue period in the same trial was subtracted to calculate the reference.

(3) The labeled datasets of the cue and GVS periods were randomized, respectively, with 80% defined as the training data and the remaining 20% as the test data.

(4) The absolute magnitude[20] of the randomized data was cut off at intervals of the 0.5 s decoding time window (GVS at 0–0.1 s, 0.1–0.2 s, 0.2–0.3 s, 0.3–0.4 s, 0.4–0.5 s, for each 100 ms period: 51 features/channel) as the training feature and test feature matrices.

(5) The training and test feature matrices with the corresponding label vectors were sent decoded, and the classification accuracies of training/test data and weight vector were obtained.

(6) Steps (3)–(5) were repeated 20 times; then, the classification accuracies of the training/test data and weight vectors were all saved. After that, the subsequent program could analyze the statistical results and conduct the channel screening.

As it is parameter-free and robust against overfitting,[38] sparse logistic regression (SLR) was used to classify the EEG data. It provides a solution for binary or multiclass classification. A binary decoder, SLR with variational approximation (SLR-VAR), was utilized in this study. In the algorithm, the weight of the uncorrelated feature of decoding was set to zero and the weight of the associated feature was set to a nonzero value. The feature matrix and label vector of the training and test data should be entered into the decoder to acquire the weight vector and decoding accuracy matrix.

2.6. *Channel screening*

Since the prediction error decoding utilized in this study showed satisfactory performance in the front/back MI task during the 0.5 s GVS period

(see the red portion in Fig. 4), we further proposed a channel screening method based on the weight parameters (WPS), and hoped to reduce redundant information channels while maintaining or improving the original decoding performance.

After the EEG data were analyzed and classified using the SLR-VAR algorithm, the weight vectors of all the channels could be acquired. In this research, each participant had 64 EEG measurement channels and five object decoding time windows (each time window was 100 ms, containing 51 features) that were classified 20 times; hence, the initial weight parameter vector was structured as [(64 channels × 51 features corresponding weight parameters) × 5 time periods × 20 rounds of decoding].

As previously mentioned, the weight of the uncorrelated feature was set to zero and the weight of the associated feature was set to a nonzero value in the SLR algorithm. Therefore, the nonzero values of the initial weight parameter vector were counted, and the count values of 20 rounds were summed and averaged across five time periods; hence, a comprehensive count vector that was structured as [64 channels × 1 comprehensive count value] could be calculated. Then, the vector was sorted in descending order, and the top number of channels was selected and processed for each participant individually (called individual-selected mode).

After that, different participants would obtain different descending ordered channels; however, the diversity of the object selected channel was not conducive to future commercial applications. Hence, the common-selected mode was investigated. The comprehensive count vectors of the 10 participants were averaged and sorted in descending order. The count values of all 64 channels are plotted in a bar graph, and the distribution is mapped on a brain layout. The top number of common-selected channels was selected and analyzed for all 10 participants, and the comprehensive decoding performance was evaluated with the individual-selected mode. Additionally, a CCS method proposed in other studies[36,37] was also compared with the WPS method (under the common-selected mode and across the participants). This method conducted a Pearson's correlation analysis of the EEG data between each pair of channels and then combined the correlation coefficients between each channel and all the others to obtain the comprehensive mean correlation coefficient vector of all 64 channels. Then, the channels were sorted in descending order, and the highly correlated channels were selected.

3. Results

Ten participants were involved in the experiments in this study. The participants were asked to sit on a revolving chair in a shielded room in a quiescent state (keep the eyes closed and body still) and were cued with an audio signal from two speakers that were placed on either side of the participant. They were required to imagine thoughts similar to the actual motion control of the wheelchair after listening to the cues. Three seconds after the end of the cues, GVS (attached to the left/right side temples and mastoids, see Fig. 2(a)) was applied to induce the vestibular sensation of the left, right, forward, and backward (see timeline in Fig. 3(a)), which was associated with the generation of prediction errors. The participants EEG signals were recorded throughout the experiment (see the detailed procedures in the Materials and Methods).

3.1. *Intentional decoding*

The intention decoding section (cue period) only contains the motor imagination data according to the direction of the audio cues. The brain wave was recorded and aligned with the ending of the cue presentation. The data were divided according to whether the cue direction was front or back. In the hypothetical wheelchair control method, the decoding time window was set to 100 ms, therefore, we divided the EEG data of the 3 s period of pure MI into 30 equal parts. It should be noted that 80% of these data were used for training and the remaining 20% were used for testing. The process was repeated 20 times for a comprehensive analysis of the decoding performance.

The brain activity of the cue period (see the decoding performance represented by the blue color in Fig. 4) was based solely on the MI (front/back). It can be seen that the decoding accuracy was mainly distributed around the chance level ($H = 0$, $P = 0.96$; the decoding rates of all the cue periods across the participants were analyzed by the one-sample t-test). The results of different decoding time windows showed a stable low decoding rate ($F = 0.97$, $P > 0.05$, one-way ANOVA) in the cue period.

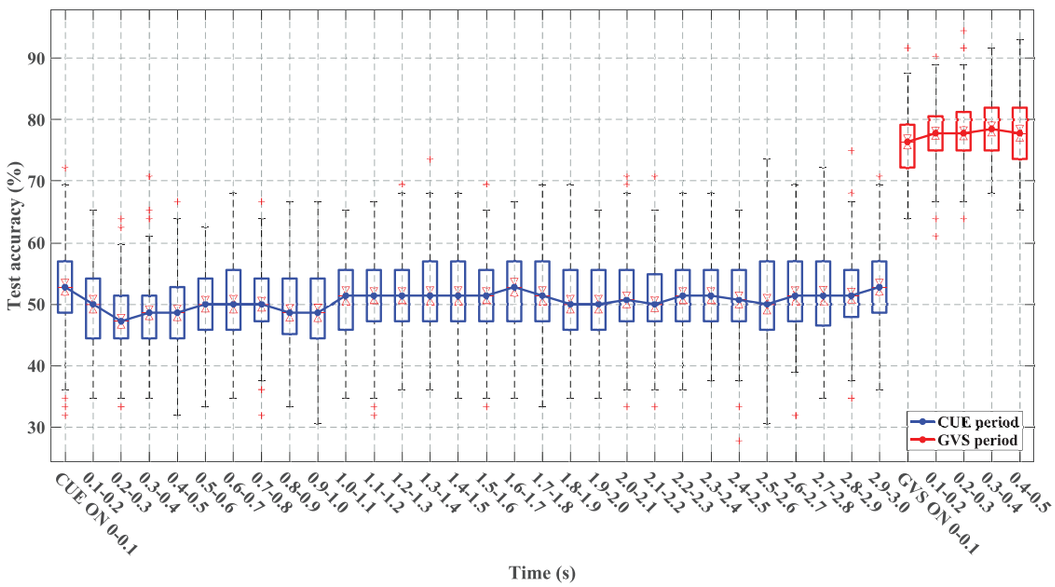

Fig. 4. (Color online) Box plot-line chart of the decoding accuracy across participants: all the participants decoding performances in the 0–3 s cue period and 0–0.5 s GVS period (the data were analyzed each 100 ms for a total of 35 periods. Each contained the results of 10 participants and 20 rounds of decoding) were combined and plotted. Each boxplot represents the performance of 20 rounds of decoding for all the tested participants, and the line graph connects the median values. The blue and red graphs represent the cue and GVS periods, respectively.

3.2. *Prediction error decoding*

In the 0–0.5 s GVS period, the EEG data were recorded and were aligned with the start time of the GVS. The prediction errors were decoded according to whether the direction of the MI was equal to the induced sensory feedback of the GVS: MATCH (the cue and GVS directions corresponded) and MISMATCH (the cue and GVS directions did not correspond).

Figure 4 shows that the decoding performance achieved in the GVS period is significantly superior to that of the cue period ($F = 2049.12$, $P < 0.01$, one-way ANOVA) and chance level ($H = 1$, $P < 0.01$, one-sample t-test). The median decoding accuracy of the first 100 ms was 76.4% (ranging between 72.2% and 91.7%), and the median accuracy of the entire GVS period was 76%79%, and the decoding performance remains similar thereafter ($P > 0.05$, one-way repeated-measures ANOVA). Some participants results exceeded 90% (Participants 3, 8 and 10). The results revealed that the proposed method achieved a satisfactory decoding performance for the prediction errors in the MI of the front/back.

3.3. *Proposed channel screening method: WPS*

Multichannel EEG signals are widely used for acquiring brain activity data in BCI. Although the prediction error decoding showed satisfactory performance during the GVS period, redundant information may have been recorded on some channels, which influenced the decoding performance. Additionally, to adapt real-time control in future studies, only channels that are highly relevant to the decoding should be selected. A channel screening method based on weight parameters (WPS) was proposed in this research.

In the WPS individual-selected mode, the nonzero value of the weight parameters in each channel was counted after the EEG data were analyzed, and then all the channels were sorted in descending order of count values (see channel screening in Materials and Methods in detail). The top 32 channels were first selected and analyzed and then we halved the number of channels successively and attempted to select and decode the top 16 channels, 8 channels and 4 channels (a total of four selection types)

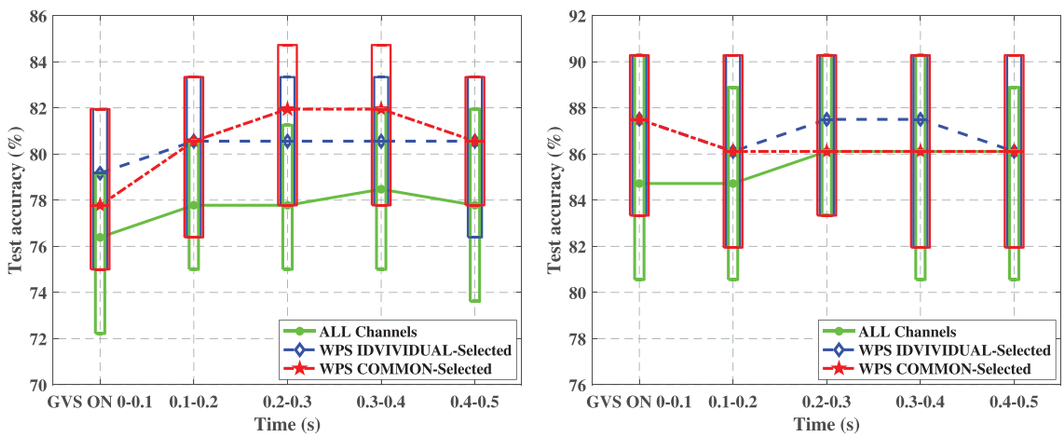

(a) (b)

Fig. 5. (Color online) Comparison of the decoding performance for different channel selection modes of WPS during the GVS period. (a) Channel screening in prediction error decoding of the front/back MI task; (b) Channel screening in prediction error decoding of the left/right MI task. The decoding performance (across 10 participants) of all the channels (green), WPS individual-selected mode (blue), and WPS common-selected mode (red) were plotted in the figure. The line graph connected the median value of each section. The abscissa represents the periods, and the ordinate represents the test decoding accuracy.

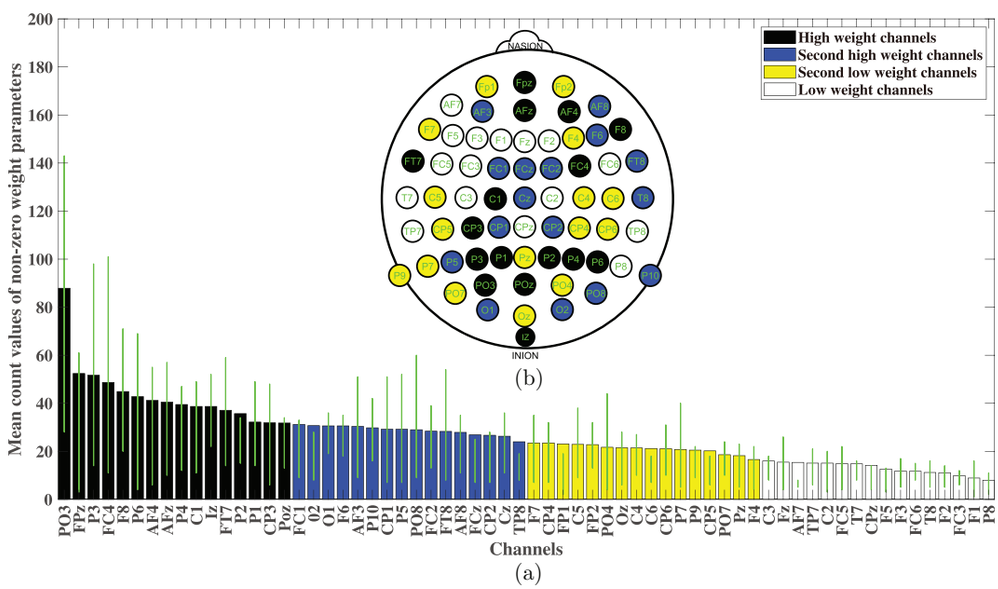

(b)

(a)

Fig. 6. (Color online) Bar chart and spatial distribution of nonzero weight mean count values across participants. The WPS-processed channels were sorted in descending order and were tentatively categorized into four classes: high weight channels (black), second high weight channels (blue), second low weight channels (yellow) and low weight channels (white). The distribution of the count values (all 10 participants) are exhibited (green line). The abscissa represents channel names, and the ordinate represents the mean count values.

for each participant. The comprehensive decoding performances of the WPS individual-selected mode (containing all four selection types) is shown in Fig. 5 (blue graph).

Nevertheless, the diversity of the selected channels was not conducive to future common applications. Hence, the count values of all 64 channels across the participants were averaged, combined and arranged in descending order (WPS common-selected mode) and plotted in Fig. 6(a). The spatial distribution is shown in Fig. 6(b). This shows the spatial distribution of the weight parameters in terms of relevancy to the prediction error decoding. However, the feature selection of the decoder is prone to false negatives, and in this study, the use of 0 as the counting threshold of the weight parameters is explored; hence, further concrete deductions regarding the spatial distribution of the underlying neural mechanism from the nonzero weight parameters selected by the decoder cannot be made. However, some information can still be obtained. Many darker electrodes are distributed over the parietal lobe, which is closely related to spatial information processing. Although the remaining darker electrodes are distributed in areas that do not closely correspond to MI, these channels are highly related to decoding.

Similar to the verification in the WPS individual-selected mode, we also selected and analyzed the first 32, 16, 8 and 4 channels (a total of four selection types) according to the descending order of common channels across the participants. The decoding performance of the WPS common-selected mode (containing all four selection types) is plotted in Fig. 5 (red graph).

The above content was verified first for the front/back MI task and then the left/right MI task. The average decoding accuracy of all 10 participants

Table 1. Average decoding accuracy (%) of all 10 participants (GVS period) of all channels, WPS individual-selected mode and WPS common-selected mode. The standard deviation is shown in parentheses.

Front/back MI task

Participants	All channels	WPS individual-selected mode	WPS common-selected mode
1	76.19 (±5.17)	78.69 (±4.71)	78.40 (±4.71)
2	76.19 (±4.56)	78.02 (±4.77)	78.57 (±4.69)
3	78.13 (±4.30)	81.49 (±4.59)	81.28 (±4.40)
4	79.07 (±5.67)	81.34 (±4.59)	81.91 (±4.49)
5	77.64 (±4.72)	80.17 (±4.38)	81.62 (±5.04)
6	75.83 (±4.74)	78.87 (±4.59)	79.49 (±4.92)
7	77.46 (±4.93)	80.05 (±4.72)	80.64 (±4.99)
8	79.00 (±4.46)	80.28 (±4.70)	80.64 (±4.77)
9	77.61 (±4.73)	79.49 (±4.69)	80.24 (±4.84)
10	79.78 (±4.53)	81.10 (±4.15)	80.85 (±4.41)

Left/right MI task

Participants	All channels	WPS individual-selected mode	WPS common-selected mode
1	76.90 (±4.10)	79.98 (±4.71)	80.29 (±4.86)
2	82.25 (±4.15)	82.03 (±4.64)	83.15 (±4.11)
3	94.39 (±2.86)	94.22 (±2.73)	94.25 (±2.75)
4	80.96 (±4.04)	82.76 (±4.19)	82.86 (±4.07)
5	87.57 (±4.72)	88.77 (±4.03)	87.40 (±4.05)
6	83.57 (±3.91)	84.47 (±4.06)	83.99 (±4.07)
7	90.24 (±2.65)	90.11 (±3.75)	91.05 (±3.39)
8	85.03 (±3.76)	85.95 (±3.96)	84.61 (±4.03)
9	87.86 (±4.04)	88.05 (±3.66)	86.52 (±4.24)
10	86.26 (±2.97)	87.61 (±3.77)	87.77 (±4.06)

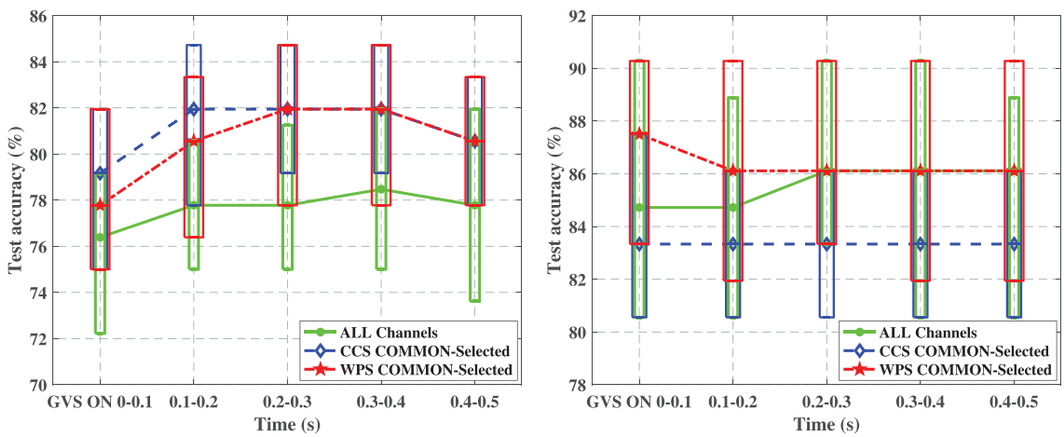

Fig. 7. (Color online) Comparison of the common-selected modes of WPS and CCS during the GVS period. (a) Channel screening in prediction error decoding of the front/back MI task; (b) Channel screening in prediction error decoding of the left/right MI task. The decoding performance (across all 10 participants) of all channels (green), WPS common-selected mode (red) and CCS common-selected mode (blue) were plotted in this figure. The line graph connected the median value of each section. The abscissa represents the periods, and the ordinate represents the test decoding accuracy.

of all the channels, WPS individual-selected mode, and WPS common-selected mode (across five GVS periods and four selection types) are shown in Table 1.

3.4. *Another channel screening method: CCS*

The channels related to MI may contain common information when participants are executing the corresponding tasks.[36] Based on this hypothesis, a CCS method was proposed in a previous study to select channels that contained more correlated information. The performances of WPS and CCS were compared in the common-selected mode (analysis across participants, MI task of front/back and left/right side, during the GVS period). Similar to the WPS, we also selected and analyzed the highly correlated 32, 16, 8 and 4 channels (a total of four selection types) for all participants. The decoding performances (containing all four selection types) of the WPS (red) and CCS (blue) are plotted in Fig. 7.

As shown in Fig. 7(a), for the front/back MI task, the WPS-based channels and CCS-based channels have better decoding performance than all the channels ($p < 0.01$, two-sample t-test; the decoding performance across 10 participants and four selection types were compared), but there was no significant statistical difference between the decoding performance of the WPS and CCS methods ($p > 0.05$, except for the 0.2–0.4 s GVS period, two-sample t-test). However, in the left/right MI task (see Fig. 7(b)), although a significant statistical difference between the decoding performance of WPS and all channels could not be observed ($p > 0.05$, except for the 0–0.2 s GVS period, two-sample t-test), the decoding performance of WPS was superior to that of CCS ($p < 0.01$, two-sample t-test). Furthermore, the decoding accuracy of the CCS method was even lower than that of all the channels ($p < 0.01$, two-sample t-test).

4. Discussion

The BCI is used to translate brain activity into a command for the computer or machine.[3,39] In recent years, to improve the decoding performance and feasibility of BCI systems, many schemes have been proposed. A fusion approach that combines EEG and magnetoencephalography (MEG) simultaneously was proposed to improve the decoding performance.[40] However, MEG systems are bulky and expensive, making them difficult to implement on mobile BCI. The generalization ability of classifiers in BCI was improved in a previous study,[41] and the results demonstrated comparable performance improvement across multiple subjects without subject-specific calibration. A flexible group sparse

discriminative analysis algorithm based on Moreau–Yosida regularization was proposed to improve the event-related potential (ERP) classification problem in a study.[42] P300 is a type of ERP, which is a special endogenous evoked potential related to cognitive function. Some typical researches decoded it via continuous tapping of the finger and thumb[43] and also via left-hand and right-hand movement MI,[44] which is different from the MI of the actual control task. In addition, the latency of P300 is not accurate (250–800 ms), making it difficult to obtain satisfactory decoding accuracy in a short period of less than 300 ms. One study[45] verified that visuospatial imagery could be used to signify intent in an online EEG-based BCI. In another study[46] based on effective spatial filtering algorithm in steady state visually evoked potentials (SSVEP)-based BCIs, a novel canonical correlation analysis (CCA) method is proposed in which spatial filters are estimated using training data only, the robustness of CCA to noise shows potential in practical applications. The characteristics of the analytic common spatial patterns (CSP) method have been detailed and investigated in a previous study.[47] The spatial model of this method is composed of amplitude and phase components that provide a more comprehensive understanding of basic activities and relatively good analytical performance in the SSVEP system but require more electrodes to enrich the characteristic structure for decoding brain activity. The decoding algorithm used in this study is more inclined to reduce the weight of the uncorrelated feature of decoding, which also provides the conditions for our subsequent channel screening. Although the proposed methods have exhibited good decoding performance, some of them may require either a complex algorithm or high experimental cost. By analyzing the GVS-induced prediction errors, the method proposed in this paper can significantly improve the decoding accuracy using the common algorithm and will not increase the load of experiment and decoding.

4.1. *Direct intention decoding and prediction error decoding*

The results of the front/back MI task indicated that the decoding performance of the GVS period (containing prediction errors of all 64 channels) was significantly superior to that of the cue period (containing direction intention). The mean improvement of decoding accuracy between the 0–0.5 s cue and the 0–0.5 s GVS period was 28.56% (std = 2.60, $p < 0.01$, two-sample t-test). The test decoding accuracy reached 77.83% to 78.86% (mean) during the GVS period, and some specific participants 90.3% (Participant 3), 91.7% (Participants 1, 10), 93.1% (Participant 8) and 94.4% (Participant 3). Additionally, the proposed method was also verified for the left/right MI task, whereas a median decoding accuracy range of 86–87% was observed for each 100 ms during the GVS period (was similar to the results in our previous study). As seen, prediction errors are a good indirect means of decoding MI.

In this research, the SLR algorithm was used to decode the EEGs directional intention data and prediction errors. It has the advantages of being parameter-free and robust to overfitting, but it also contains problems such as over-pruning features[48]; hence, using other algorithms may improve the decoding performance. It was verified in our previous research[20] using a support vector machine and iterative SLR,[48] and the results revealed that the decoding performance was similar.

4.2. *GVS and its artifacts in the decoding*

Validation of the GVS-induced degree of stimulation was implemented in a previous study. According to the statistical results of reported comprehensive sensory levels (including vestibular perturbation, muscle twitch and tactile sensation), GVS with a current value of 0.8 mA and below would not cause current tingling (the tingling could be attenuated by shaving the hair under the GVS electrodes and wetting the skin with a swab). In this research, a maximum current of 0.4 mA of insensible subliminal stimulus was used on the participants. According to the results of the GVS perception questionnaire, participant reports were 1 (1 represents no feeling) for the comprehensive GVS stimulus at the amplitude of GVS (0.4 mA) used in our experiment to ensure that the stimulus was subliminal.

The satisfactory decoding performance verified that the lower GVS intensity induced prediction errors could acquire a reliable decoding performance and ensure no usage burdens of the hypothetical EEG-controlled wheelchair. As the stimulus intensity

in this study was lower than that of the previous study, we could obtain a satisfactory decoding performance, indicating that the lower current intensity also induced subconscious stimuli very well. In a follow-up study, we will investigate the lowest threshold current value of subconscious stimulation.

GVS artifacts are another matter that is easy to consider. According to our previous study[20] to verify whether GVS artifacts affect decoding, experiments that were similar to the main experiment except for the GVS location were conducted. GVS electrodes were attached to the forehead and the back of the neck not to correspond properly with the direction of MI. Although all tasks were mismatched, two kinds of trials were forcibly marked MATCH and the other two were forcibly marked MISMATCH. The decoding process was similar to that of the main experiment. The results showed that the prediction error decoding was significantly less than the case when the GVS corresponded to the direction of MI, but a strong correlation was observed between the EEG channel weights chosen by the decoder in the verification experiment and those chosen in the main experiment. These results comprehensively suggest that GVS artifacts do not affect decoding.

4.3. *Comparing the individual-selected mode and common-selected mode of WPS*

In Fig. 5, the decoding performance of all channels is shown in green. It can be seen from Fig. 5(a) (front/back MI task) that the decoding performance of the individual-selected mode/common-selected mode was better than that of all channels ($p < 0.01$, two-sample t-test; the decoding performance across four selection types and 10 participants were compared). Although the difference between the common-selected mode and individual-selected mode was not statistically significant ($p > 0.05$, two-sample t-test), a slight improvement was observed. In Fig. 5(b) (left/right MI task), after the individual-selected mode/common-selected mode of WPS was utilized, the performance was slightly improved ($p < 0.05$, except 0.2–0.3 s GVS period, two-sample t-test), but there was also no significant statistical difference between the performance of the two modes ($p > 0.05$, two-sample t-test). In summary, the proposed WPS is an alternative method for reducing redundant channels, and the WPS common-selected mode can choose common and fewer channels to obtain a decoding performance similar to that of the individual-selected mode, which is also a desirable option.

4.4. *Comparing the two different channel screening methods: WPS and CCS*

Although the data from all channels for decoding could maximally ensure the use of all potentially useful information, to a certain extent, it would also reduce the decoding efficiency owing to the inclusion of redundant information that was not conducive to future practical conversion in some channels.

A channel screening method based on the count values of the weight parameters (WPS) was proposed in this research. The weight vectors of all the channels could be acquired after decoding. The nonzero values of the weight parameter vector (across the 5 GVS data processing period and 20 rounds of testing) were counted, and the count values of 64 channels were summed and sorted in descending order for each participant separately (WPS individual-selected mode). The top channels were considered to be highly related to decoding, and they were selected for further analysis. Satisfactory decoding performance was achieved. Additionally, to explore whether it was possible to select channels with "commonality" for all participants, the count values of 64 channels were comprehensively analyzed and ranked across participants (WPS common-selected mode). Likewise, the top common-selected channels were analyzed for all participants. These channels also showed satisfactory decoding results across participants, which proved the effectiveness and feasibility of the WPS method.

In the CCS method used for comparison, Pearson correlation analysis on EEG data between each pair of channels was performed, and the correlation coefficients between each channel and all other channels were combined to obtain the comprehensive average correlation coefficient vector of all 64 channels. Similarly, the channels are sorted in descending order, and highly correlated channels are selected.

As shown in Fig. 7, the decoding performance of CCS and our proposed WPS was similar, and WPS performed better in the channel screening of prediction error decoding in the left/right MI task. WPS and CCS did not significantly improve the decoding

accuracy even though they undoubtedly reduced the number of channels required for decoding because the GVS-induced prediction errors greatly increased the decoding rate. Therefore, further channel selection could only be improved to a limited extent. Furthermore, the advantage of the CCS method is that it can directly select the highly correlated channels before data processing, while the WPS requires the weight vector obtained after data processing to perform channel selection. In addition, the analysis of the weight parameters was based on nonzero values; therefore, it is necessary to explore the influence of other fiducial values and optimize the entire selection mechanism.

In general, during channel screening, the channels with considerable redundant information could be eliminated, and other channels that are more relevant to decoding could be selected. As shown, channel screening could improve or maintain decoding performance while reducing the experimental load and decoding cost.

4.5. *Future plans*

(1) Apply the proposed GVS-induced prediction error decoding method to the EEG-controlled wheelchair.
(2) Explore the current threshold of GVS-induced subconscious stimulation.
(3) Utilize opposite directional anteroposterior stimulation (another GVS pattern)[35] to induce left and right yaw, which is similar to the MI content of left and right rotation, and compare the decoding performance of the prediction error that was induced by LDS (left and right roll).

5. Conclusion

In this study, first, the decoding performance of the galvanic vestibular stimulation (GVS) induced prediction errors in the forward and backward directions was verified. Second, a weight parameter-based channel screening (WPS) method was proposed and verified. The experimental results suggest that the prediction errors induced by the GVS can be effectively decoded in the front/back motor imagery (MI) task, and that the WPS method can be used to select channels that are highly related to decoding, reducing redundant channels.

Acknowledgments

This work was supported in part by JSPS under Grant No. KAKENHI 18H04109 and JST PRESTO (Precursory Research for Embryonic Science and Technology; Grant No. JPMJPR17JA).

References

1. A. B. Benevides, T. F. Bastos and M. Sarcinelli Filho, Proposal of brain-computer interface architecture to command a robotic wheelchair, *Proc. IEEE Int. Symp. Industrial Electronics* (2011), pp. 2249–2254.
2. S. K. Swee, K. D. Teck Kiang, L. Z. You, M. N. Tamin and R. Du, EEG controlled wheelchair, *MATEC Web Conf.* **51** (2016) 02011.
3. A. Ortiz-Rosario and H. Adeli, Brain-computer interface technologies: From signal to action, *Rev. Neurosci.* **24**(5) (2013) 537–552.
4. B. Rebsamen, C. Guan, H. Zhang, C. Wang, C. Teo, M. H. Ang and E. Burdet, A brain controlled wheelchair to navigate in familiar environments, *IEEE Trans. Neural Syst. Rehabil. Eng.* **18**(6) (2010) 590–598.
5. A. Ortiz-Rosario, I. Berrios-Torres, H. Adeli and J. A. Buford, Combined corticospinal and reticulospinal effects on upper limb muscles, *Neurosci. Lett.* **561** (2014) 30–34.
6. A. Burns, H. Adeli and J. A. Buford, Brain-computer interface after nervous system injury, *Neuroscientist* **20**(6) (2014) 639–651.
7. J. R. Wolpaw, N. Birbaumer, D. J. McFarland, G. Pfurtscheller and T. M. Vaughan, Brain–computer interfaces for communication and control, *Clin. Neurophysiol.* **113**(6) (2002) 767–791.
8. A. Shakeel, M. S. Navid, M. N. Anwar, S. Mazhar, M. Jochumsen and I. K. Niazi, A review of techniques for detection of movement intention using movement-related cortical potentials, *Comput. Math. Methods Med.* **2015** (2015) 346217.
9. G. R. Müller-Putz, A. Schwarz, J. Pereira and P. Ofner, From classic motor imagery to complex movement intention decoding: The noninvasive Graz-BCI approach, *Progress in Brain Research*, Vol. 228 (Elsevier, 2016), pp. 39–70.
10. G. Townsend and V. Platsko, Pushing the p300-based brain–computer interface beyond 100 bpm: Extending performance guided constraints into the temporal domain, *J. Neural Eng.* **13**(2) (2016) 026024.
11. M. Middendorf, G. McMillan, G. Calhoun and K. S. Jones, Brain-computer interfaces based on the steady-state visual-evoked response, *IEEE Trans. Rehabil. Eng.* **8**(2) (2000) 211–214.
12. X. Gao, D. Xu, M. Cheng and S. Gao, A BCI-based environmental controller for the motion-disabled,

IEEE Trans. Neural Syst. Rehabil. Eng. **11**(2) (2003) 137–140.
13. L. O'hare, Steady-state VEP responses to uncomfortable stimuli, *Eur. J. Neurosci.* **45**(3) (2017) 410–422.
14. K. Dremstrup, Y. Gu, O. Nascimento and D. Farina, Movement-related cortical potentials and their application in brain-computer interfacing, *Introduction to Neural Engineering for Motor Rehabilitation* (John Wiley & Sons, 2013), pp. 253–266.
15. N. Birbaumer, A. Kubler, N. Ghanayim, T. Hinterberger, J. Perelmouter, J. Kaiser, I. Iversen, B. Kotchoubey, N. Neumann and H. Flor, The thought translation device (TTD) for completely paralyzed patients, *IEEE Trans. Rehabil. Eng.* **8**(2) (2000) 190–193.
16. N. Birbaumer, T. Elbert, A. G. Canavan and B. Rockstroh, Slow potentials of the cerebral cortex and behavior, *Physiol. Rev.* **70**(1) (1990) 1–41.
17. L. A. Miner, D. J. McFarland and J. R. Wolpaw, Answering questions with an electroencephalogram-based brain-computer interface, *Arch. Phys. Med. Rehabil.* **79**(9) (1998) 1029–1033.
18. J. R. Wolpaw, H. Ramoser, D. J. McFarland and G. Pfurtscheller, EEG-based communication: Improved accuracy by response verification, *IEEE Trans. Rehabil. Eng.* **6**(3) (1998) 326–333.
19. M. Z. Al-Faiz and A. A. Al-Hamadani, Implementation of EEG signal processing and decoding for two-class motor imagery data, *Biomed. Eng.: Appl. Basis Commun.* **31**(4) (2019) 1950028.
20. G. Ganesh, K. Nakamura, S. Saetia, A. M. Tobar, E. Yoshida, H. Ando, N. Yoshimura and Y. Koike, Utilizing sensory prediction errors for movement intention decoding: A new methodology, *Sci. Adv.* **4**(5) (2018) eaaq0183.
21. D. M. Wolpert and J. R. Flanagan, Motor prediction, *Curr. Biol.* **11**(18) (2001) R729–R732.
22. X. Tian and D. Poeppel, Mental imagery of speech and movement implicates the dynamics of internal forward models, *Front. Psychol.* **1** (2010) 166.
23. R. Gentili, C. E. Han, N. Schweighofer and C. Papaxanthis, Motor learning without doing: Trial-by-trial improvement in motor performance during mental training, *J. Neurophysiol.* **104**(2) (2010) 774–783.
24. G. Ganesh, R. Osu and E. Naito, Feeling the force: Returning haptic signals influence effort inference during motor coordination, *Sci. Rep.* **3** (2013) 2648.
25. E. Todorov and M. I. Jordan, Optimal feedback control as a theory of motor coordination, *Nat. Neurosci.* **5**(11) (2002) 1226.
26. S.-J. Blakemore, C. D. Frith and D. M. Wolpert, Spatio-temporal prediction modulates the perception of self-produced stimuli, *J. Cogn. Neurosci.* **11**(5) (1999) 551–559.
27. Y.-W. Tseng, J. Diedrichsen, J. W. Krakauer, R. Shadmehr and A. J. Bastian, Sensory prediction errors drive cerebellum-dependent adaptation of reaching, *J. Neurophysiol.* **98**(1) (2007) 54–62.
28. A. Takagi, G. Ganesh, T. Yoshioka, M. Kawato and E. Burdet, Physically interacting individuals estimate the partners goal to enhance their movements, *Nat. Hum. Behav.* **1**(3) (2017) 0054.
29. T. Ikegami and G. Ganesh, Watching novice action degrades expert motor performance: Causation between action production and outcome prediction of observed actions by humans, *Sci. Rep.* **4** (2014) 6989.
30. T. Ikegami and G. Ganesh, Shared mechanisms in the estimation of self-generated actions and the prediction of other's actions by humans, *eNeuro* **4**(6) (2017).
31. L. Aymerich-Franch, D. Petit, A. Kheddar and G. Ganesh, Forward modelling the rubber hand: Illusion of ownership modifies motor-sensory predictions by the brain, *R. Soc. Open Sci.* **3**(8) (2016) 160407.
32. T. Maeda, H. Ando and M. Sugimoto, Virtual acceleration with galvanic vestibular stimulation in a virtual reality environment, *IEEE Proceedings. VR 2005. Virtual Reality, 2005* (2005), pp. 289–290.
33. R. C. Fitzpatrick, J. Marsden, S. R. Lord and B. L. Day, Galvanic vestibular stimulation evokes sensations of body rotation, *Neuroreport* **13**(18) (2002) 2379–2383.
34. R. C. Fitzpatrick and B. L. Day, Probing the human vestibular system with galvanic stimulation, *J. Appl. Physiol.* **96**(6) (2004) 2301–2316.
35. K. Aoyama, H. Iizuka, H. Ando and T. Maeda, Four-pole galvanic vestibular stimulation causes body sway about three axes, *Sci. Rep.* **5** (2015) 10168.
36. J. Jin, Y. Miao, I. Daly, C. Zuo, D. Hu and A. Cichocki, Correlation-based channel selection and regularized feature optimization for MI-based BCI, *Neural Netw.* **118** (2019) 262–270.
37. S. Roy, D. Rathee, K. McCreadie and G. Prasad, Channel selection improves MEG-based brain-computer interface, *2019 9th Int. IEEE/EMBS Conf. Neural Engineering* (*NER*) (2019), pp. 295–298.
38. O. Yamashita, M.-a. Sato, T. Yoshioka, F. Tong and Y. Kamitani, Sparse estimation automatically selects voxels relevant for the decoding of fMRI activity patterns, *NeuroImage* **42**(4) (2008) 1414–1429.
39. F. Lotte, M. Congedo, A. Lécuyer, F. Lamarche and B. Arnaldi, A review of classification algorithms for EEG-based brain–computer interfaces, *J. Neural Eng.* **4**(2) (2007) R1–R13.
40. M. C. Corsi, M. Chavez, D. Schwartz, L. Hugueville, A. N. Khambhati, D. S. Bassett and F. D. V. Fallani, Integrating EEG and MEG signals to improve motor imagery classification in brain-computer interfaces, *Int. J. Neural Syst.* **29**(1) (2017) 1850014.

41. P. Gaur, K. Mccreadie, R. B. Pachori, H. Wang and G. Prasad, Tangent space features-based transfer learning classification model for two-class motor imagery braincomputer interface, *Int. J. Neural Syst.* (2019).
42. Q. Wu, Y. Zhang, J. Liu, J. Sun, A. Cichocki and F. Gao, Regularized group sparse discriminant analysis for p300-based braincomputer interface, *Int. J. Neural Syst.* **29**(6) (2019) 1950002.
43. Y. M. Blokland, R. J. Vlek, B. Karaman, F. Özin, D. H. J. Thijssen, T. M. H. Eijsvogels, W. N. J. M. Colier, M. J. Floorwesterdijk, J. Bruhn and J. D. R. Farquhar, Detection of event-related desynchronization during attempted and imagined movements in tetraplegics for brain switch control, *Int. Conf. IEEE Engineering in Medicine & Biology Society* (2012), pp. 3967–3969.
44. C. Hohyun, A. Minkyu, A. Sangtae, K. Moonyoung and J. S. Chan, EEG datasets for motor imagery brain–computer interface, *Gigascience* **6**(7) (2017) 1–8.
45. F. Stojic and T. Chau, Non-specific visuospatial imagery as a novel mental task for online EEG-based BCI control, *Int. J. Neural Syst.* **30**(6) (2020) 2050026.
46. Q. Wei, S. Zhu, Y. Wang, X. Gao, H. Guo and X. Wu, A training data-driven canonical correlation analysis algorithm for designing spatial filters to enhance performance of SSVEP-Based BCIs, *Int. J. Neural Syst.* (2020).
47. O. Falzon, K. P. Camilleri and J. Muscat, The analytic common spatial patterns method for EEG-based BCI data, *J. Neural Eng.* **9**(4) (2012) 045009.
48. S. Hirose, I. Nambu and E. Naito, An empirical solution for over-pruning with a novel ensemble-learning method for fMRI decoding, *J. Neurosci. Methods* **239** (2015) 238–245.